Supporting Information

Coatable strain sensors on nonplanar surfaces

Chan Park[1], Jungmin Kim[1], Jeongbeam Kang[1], Byeongjun Lee[1], Haran Lee[1],
Cheoljeong Park[1], Jongwon Yoon[1], Chiwon Song[1], Hojoong Kim[2], Woon-Hong Yeo[2] and
Seong J. Cho*[1]

1 Department of Mechanical Engineering, Chungnam National University, 99 Daehak-ro,

Yuseong-gu, Daejeon 34134, Korea

2 George W. Woodruff School of Mechanical Engineering, Center for Human-Centric

Interfaces and Engineering, Institute for Electronics and Nanotechnology, Georgia

Institute of Technology, Atlanta, GA 30332, USA

* Corresponding Author: scho@cnu.ac.kr
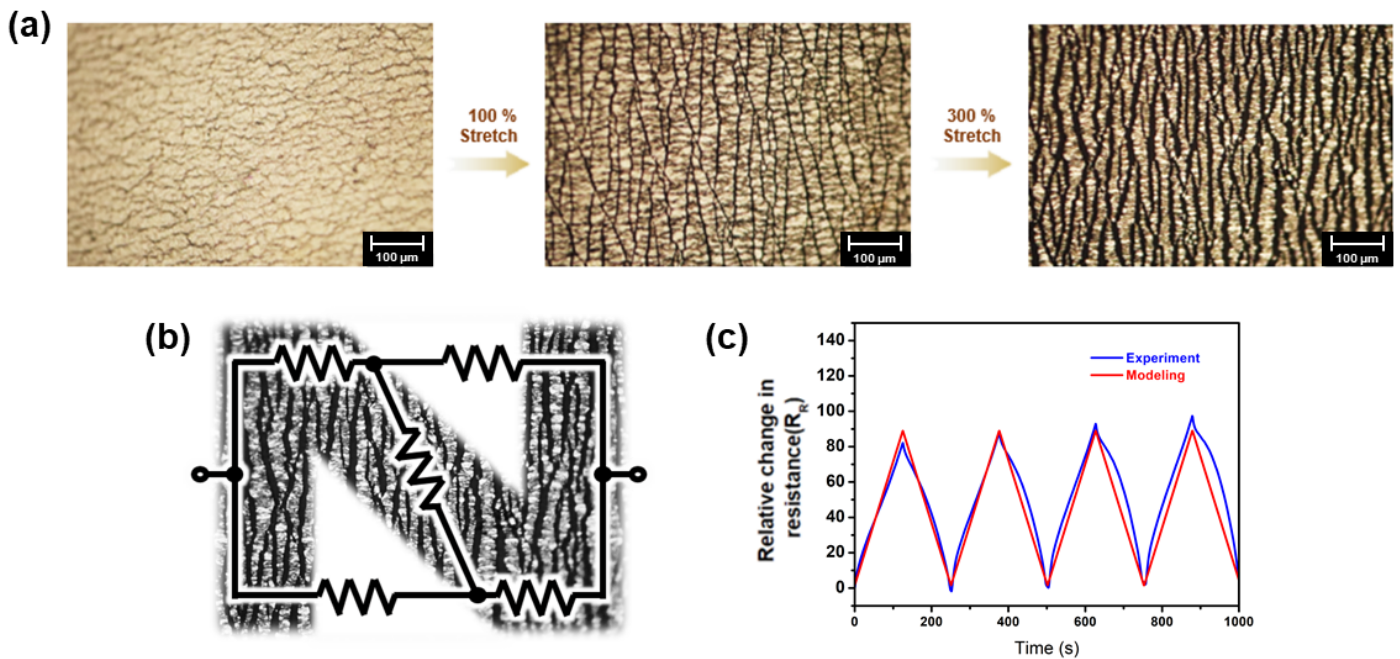
Figure S1. (a) Variation in the crack gap with initial load of up to 300% strain. (b) Model of the basic circuit of the film. (c) Comparison of analytical and experimental results in 150% strain.

SEM pictures were taken to confirm the crack generation, which is the mechanism of the crack sensor. Figure S1(a) show that the crack gap increased as the strain increased, and this was confirmed by shooting a video. Each crack is composed of a conductive metal and a crack gap and is composed of a circuit (Figure S1(b)), and the formula for calculating this was published in a previous study[1]. The calculated theoretical model and actual experimental data were compared, and they agree well with the experimental resistance change up to 150% tensile (Figure S1(c)).
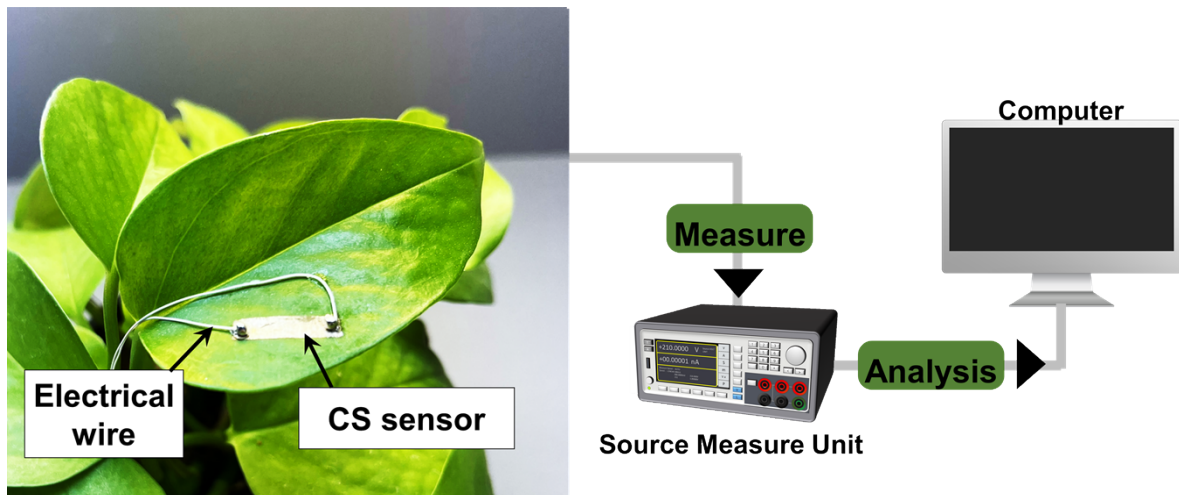
Figure S2. Digital photograph of the CS sensor fabricated on the surface of a plant leaf, connected to a Source Measure Unit for data acquisition and analysis.

Figure S2 showcases a Coatable Strain (CS) sensor fabricated directly on the surface of a plant leaf. Electrical wires connect the sensor to a Source Measure Unit (SMU), which is used to measure and analyze the sensor's output. The entire setup is designed to capture real-time data on the plant's growth and physiological changes. Given that plant leaves often have irregular and uneven surfaces, it is critical to demonstrate that the CS sensor can be uniformly fabricated on such surfaces and still maintain its functionality. This ability to conform to and operate on non-uniform, textured surfaces underscores the versatility and robustness of the CS sensor in monitoring and collecting accurate data from natural, non-planar environments.
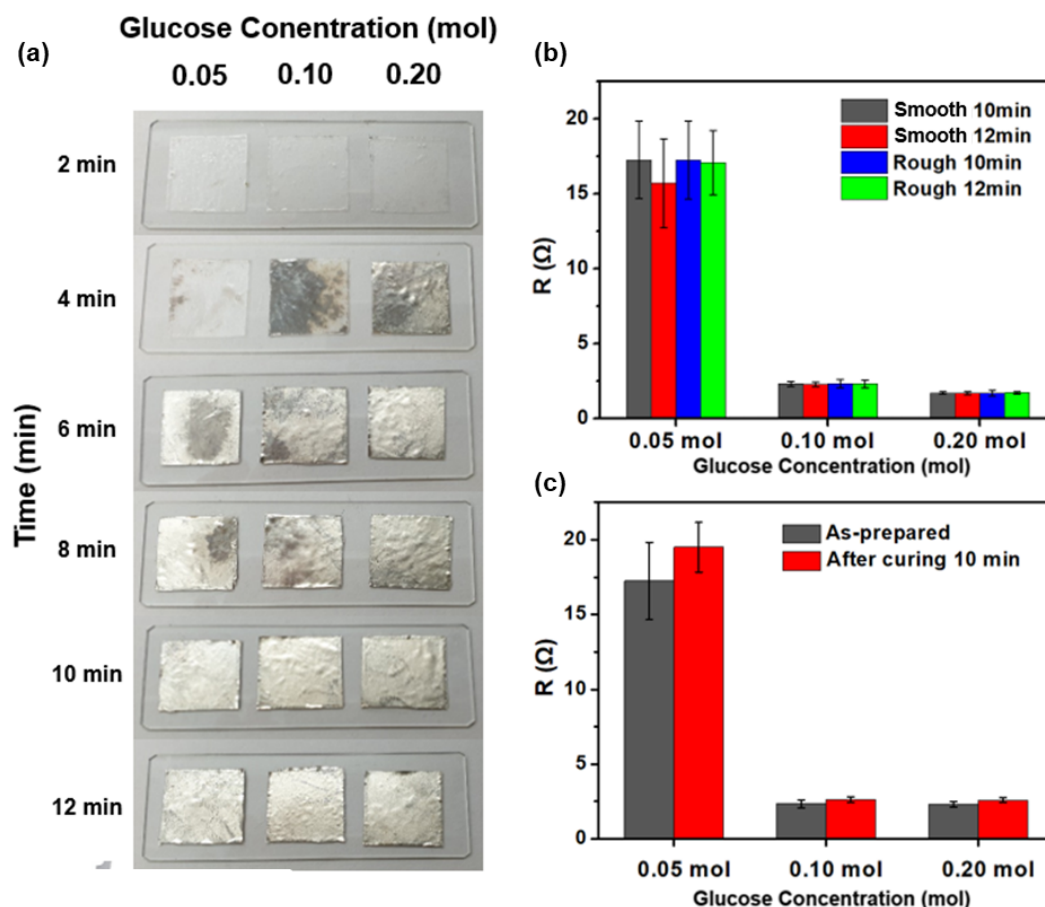
Figure S3. (a) The photographs of polymer-based CS sensor. (b) The recorded resistances of the CS sensor were prepared in 0.05, 0.10, and 0.20 mol glucose concentrations on each smooth and rough polyurethane surface (n = 5). (c) The recorded resistances of the CS sensor prepared in 0.05, 0.10, and 0.20 mol glucose concentration after placing in curing for 10 min (n = 5).

Figure S3a showed that the flat PU film became rapidly because of Tollen's solution. The changes in glucose and reaction time affected metal layer formation. The glucose concentrations of 0.05, 0.10, and 0.20 mol before 6 min showed an area where the metal layer was not formed (Figure S3). In addition, metal layers were formed at glucose concentrations of 0.05, 0.10, and 0.20 mol over 10 min. These results indicated that the smooth PU film prepared using Tollen's solution requires at least 10 min to complete the plating. An electrical evaluation was performed on both the flat and rough surfaces, and each of the four samples was measured repeatedly (Figure S3b). In Figure S3c, the moisture that remained in the wet

process is removed and checks whether the electrical conductivity changed over time, are performed.

Table S1. Comparison of performance with that in the liter

Ref.	Materials	Application (Young's Modulus)	Rough surface	Non-developable surface	Needle shape and Hairy surface	Type
26	Cr/Au - PI	Human (0.42 MPa – 0.85 MPa)	O	X	X	Thin film
30	SWCNTs - PDMS	Human (0.42 MPa – 0.85 MPa)	O	X	X	Thin film
36	Ti/Au – PI	Plant (Golden Pothos) (100 – 500 kPa)	O	O	X	Thin film
37	Au - PEN	Pig (0.9 MPa – 1.2 MPa)	O	X	X	Thin film
39	GNF - PDMS	Human (0.42 MPa – 0.85 MPa)	O	X	X	Thin film
40	GNN – PDMS	Pig (0.9 MPa – 1.2 MPa)	O	X	X	Thin film
This study	Nano Cracked silver layer – sensing materials	Hydrogel, Plant, Polymer, Concrete (> 1 kPa)	O	O	O	Coatable
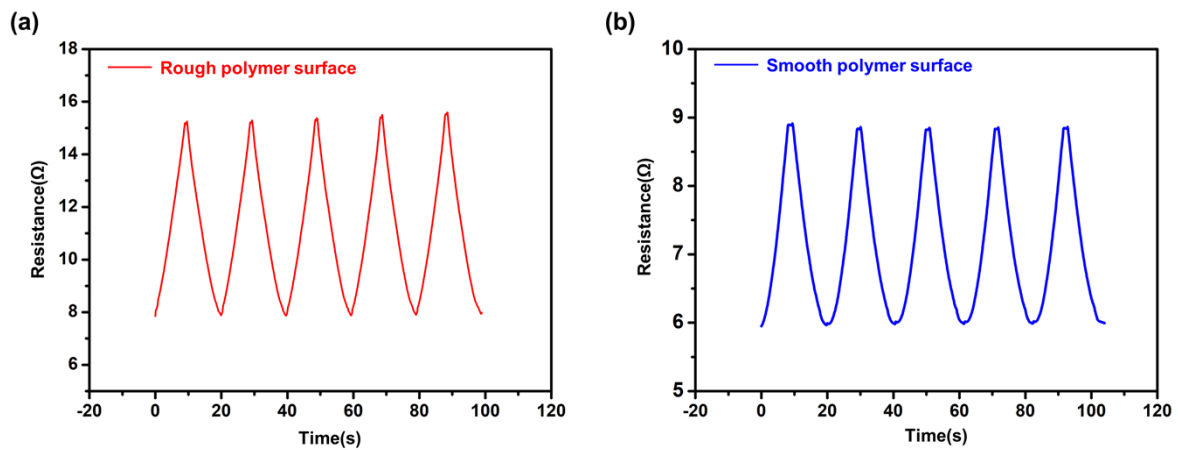
Figure S4. Performance of the polymer-based CS sensor. actual resistance changes during the cycling at the 0%–10% strain such as polymer-based (a) rough and (b) smooth surface.

Figure S4 shows the performance of the polymer-based CS sensor during cyclic tests at 1% strain. Figure S4(a) displays the resistance changes on a rough polymer surface, while Figure S4(b) shows the changes on a smooth polymer surface. The results indicate that for both rough and smooth surfaces, there is a consistent cyclic resistance change with no significant variations. However, the resistance values exhibit nonlinear characteristics around the peak and trough regions, typical of viscoelastic polymer-based sensors. This behavior, requiring a recovery time, results from the sensor's inability to immediately follow rapid movements. Despite this, the relative resistance graph aligns with the stage deformation, confirming the sensor's suitability for strain measurement.
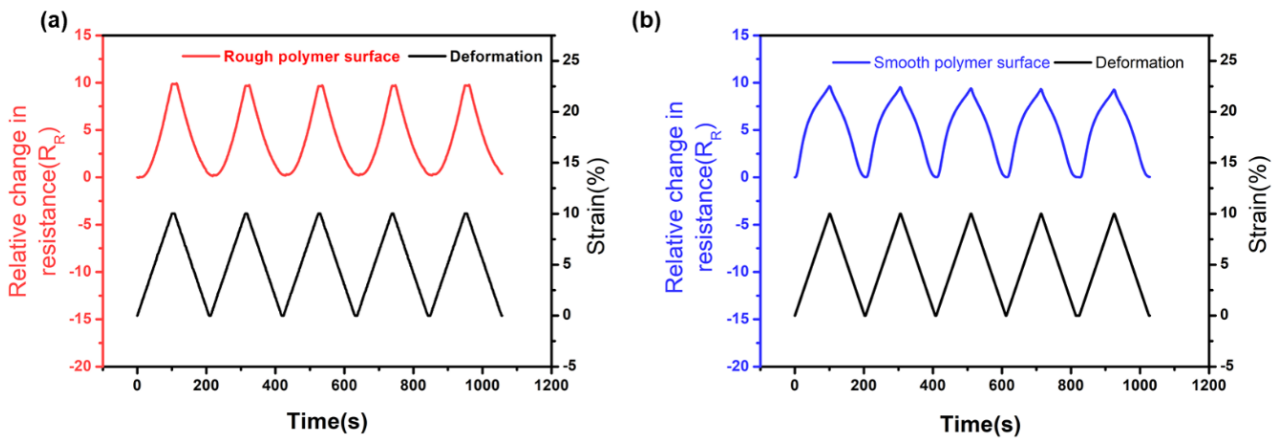
Figure S5. Performance of the polymer-based CS sensor. Relative resistance changes during the cycling at the 0%–10% strain such as polymer-based (a) rough and (b) smooth surface.

There was no significant change in resistance during repeated experiments for both rough and smooth surfaces but showed nonlinear characteristics around 0% or 10%. This is a phenomenon that, like most viscoelastic polymer-based sensors, requires a recovery time of the sensor, so it cannot follow the movement. However, because the movement of the relative resistance graph follows the deformation of the stage, it is considered suitable for use as a strain sensor.
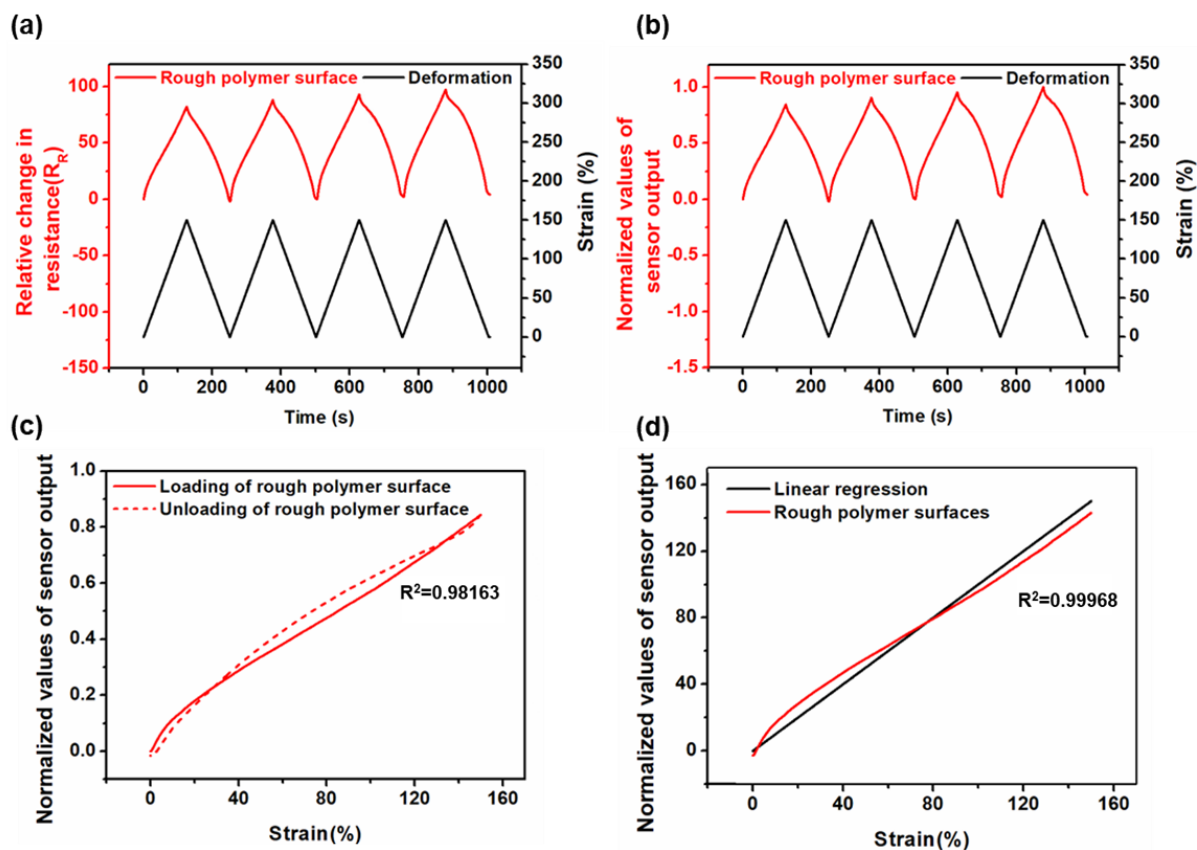
Figure S6. Performance of the CS sensor on polymer surfaces under various strain conditions. (a) Relative resistance changes during cycling from 0% to 150% strain on rough surfaces. (b) Normalized values of sensor output during the cycling from 0% to 150% strain on rough surfaces. (c) Hysteresis test at 150% strain. (d) Linearity test at 150% strain.

Figure S6 illustrates the performance of the CS sensor on polymer surfaces under 150% strain conditions. The relative resistance changes during cycling from 0% to 150% strain on rough surfaces are shown(Figure S6(a)). Although the resistance tended to increase over the four cycles, the sensor still provided distinguishable signals without waveform changes, making it potentially usable under high-strain conditions of up to 150%. To account for surface-dependent signals, the maximum R_R value was normalized to 1.0. The normalized values of the sensor output during cycling from 0% to 150% strain on rough surfaces are presented(Figure S6(b)). The normalization process ensures that the sensor can be effectively used in environments with varying surface roughness. The hysteresis test at 150% strain is also included(Figure S6(c)). As with most viscoelastic polymer-based sensors, there is a

phenomenon that it cannot follow the movement because it is not sufficiently prepared for repeated experiments, but it does tend to follow the movement of the stage. In the case of loading, it showed high linearity at 0.975, but in the case of unloading, it showed low linearity at 0.893. This is a chronic problem of viscoelastic polymer-based sensors and is expected to be materially solvable. Finally, the linearity test at 150% strain is shown(Figure S6(d)). The CS sensor exhibited excellent linearity with an R^2 value of 99.68, suggesting that it can maintain consistent performance across different levels of strain. In conclusion, while the sensor does show an increase in resistance and a tendency for the polymer to undergo plastic deformation at high strains, the ability to distinguish signals suggests that it could be made usable through further research.
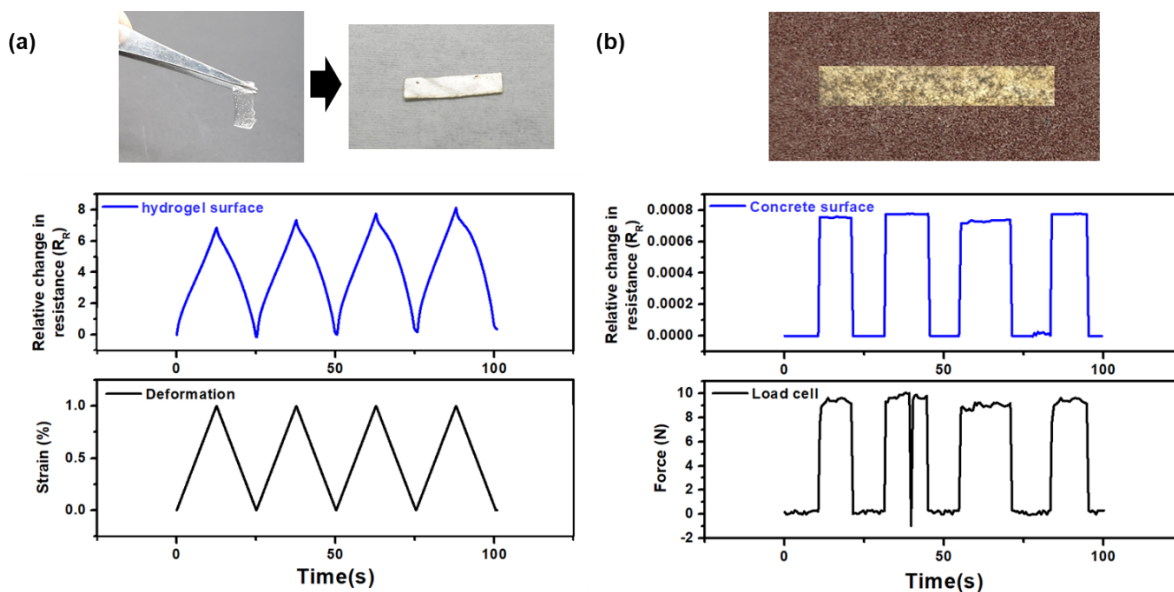
Figure S7. Performance of the CS sensor on (a) hydrogel and (b) concrete surface

Sensor evaluation was performed to confirm the applicability of CS sensors in hydrogels (Figure S7a) and concrete (Figure S7b). In the case of the hydrogel, a 1% repeated transformation was performed. Although the recovery time of the gel was delayed, there was a phenomenon that the signal was high, but the surface was coated, and the change in the signal could also be distinguished. In the case of concrete, it was difficult to deform, so it was measured with a load cell by applying a force, and the signal according to each force was distinguished, showing that the CS sensor coated on the surface can be used as a sensor.
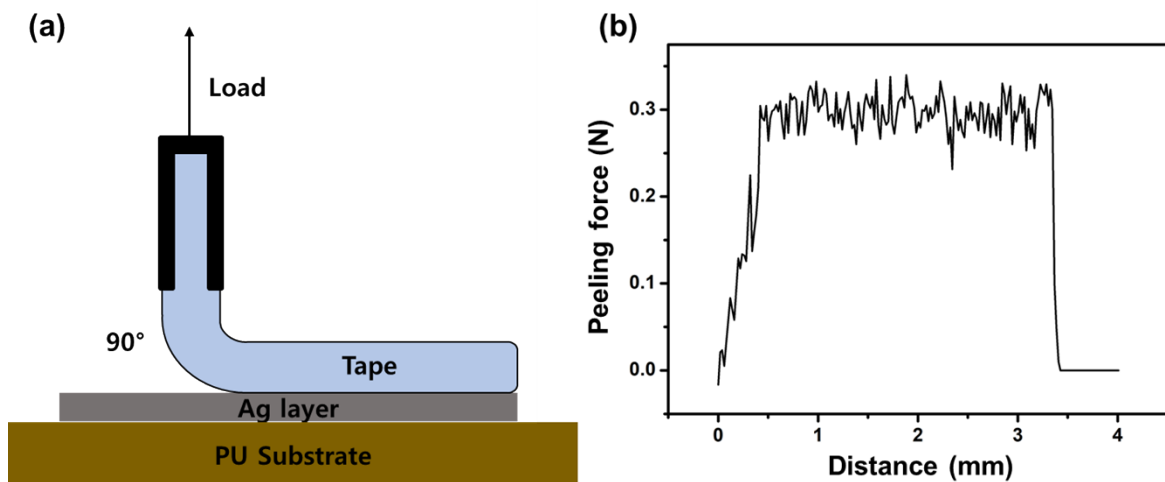
Figure S8. Peeling test of tape adhered to an Ag layer on a polyurethane (PU) substrate: (a) Test setup, (b) Graph of peeling force (N) versus peeling distance (mm).

Table S2. Resistance Changes of Ag Layer on PU Substrate after Repeated Tape Peeling Tests

	0th Cycle	1st Cycle	2nd Cycle	3rd Cycle	4th Cycle	5th Cycle
Resistance (Ω)	6.10	6.12	6.12	6.12	6.12	6.12

Figure S8 shows the results of the peeling test of 3M 467MP tape adhered to an electroless plated silver (Ag) layer on a polyurethane (PU) substrate[4]. Figure S8(a) illustrates the test setup, where the 3M 467 tape is adhered to the Ag layer and then peeled at a 90-degree angle. During this process, the peeling force was measured. Figure 8(b) presents the graph of peeling force (N) versus peeling distance (mm). The initial peeling force gradually increases to approximately 0.3 N, maintains a relatively constant value, and then sharply drops to zero as the tape completely detaches. These results indicate that the adhesive strength between the 3M 467 tape and the Ag layer remains consistent up to a certain point before abruptly failing.

Table S2 illustrates the resistance changes in the silver (Ag) layer fabricated on a polyurethane (PU) substrate after repeated tape peeling tests. The images above the table show the visual

appearance of the Ag layer on the PU substrate after each cycle. The table below displays the measured resistance (Ω) for each cycle, starting from the initial state (0th cycle) to the fifth cycle. The results indicate that the resistance remains relatively stable, with minor changes observed throughout the repeated peeling tests, demonstrating the durability and adhesion quality of the Ag layer on the PU substrate.
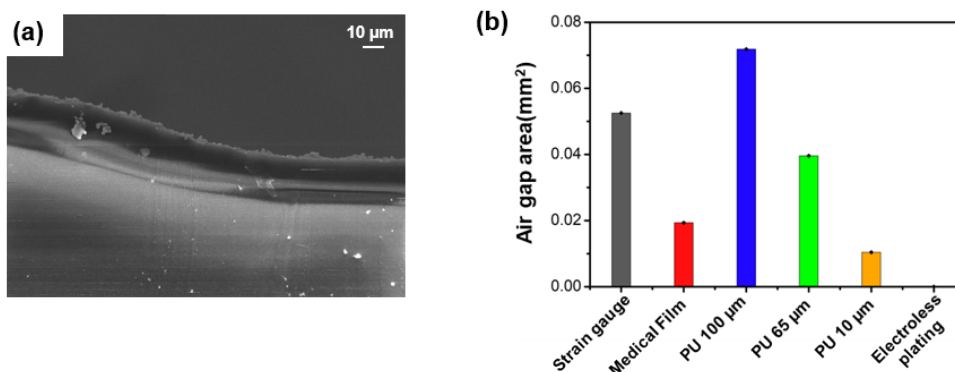
Figure S9. (a) Metal layer that maintains a constant thickness along the curved surface (b) Air gap area size existing between the surface and the film for each film type.

Metal layers fabricated on different surfaces showed a good contact area and uniform thickness (film thickness ~10 µm) regardless of surface roughness or structure (Figure S9a). A strain gauge, medical film (Tegaderm film), and PU were placed on a polymer-based rough surface and the air gap area was measured. For an accurate calculation, the area was calculated using Image J after performing SEM imaging (Figure S9b).

Table S3. Table showing the size of the air gap area present between the surface and the film for each film type.

	Control	PU 100 μm	PU 65 μm	PU 10 μm	Medical film	Strain gauge	Electroless plating
Pixel Area	91562	7985	4399	1156	2151	5837	0
Actual area(mm^2)	0.824074	0.07186644	0.0395918	0.0104042	0.019359387	0.052534051	0
Effective contact area	-	31%	45%	86%	73%	27%	100%
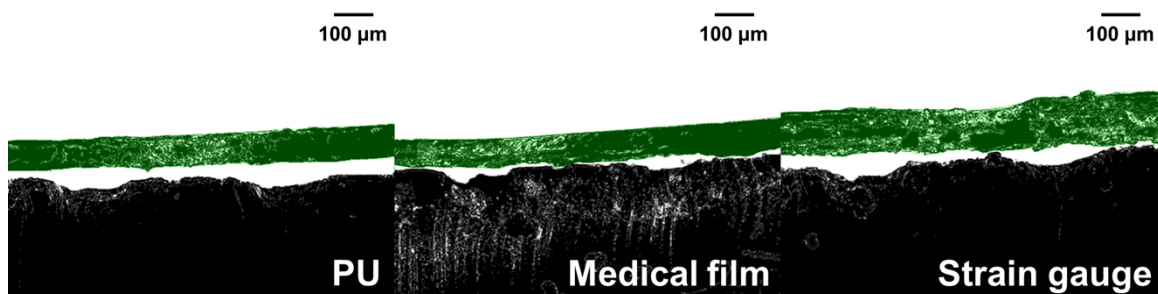
Figure S10. Cross-sectional images showing the air gap between the surface and different films: PU, Medical film, and Strain gauge.

This contact increases the effective contact area without gaps between the surfaces, which in turn increases the quality of the sensor. The optical image shown in Figure S10 was quantified to estimate the area of the efficient contact area and the results obtained are as follows (Table S2): PU 100 μm (31%), PU 65 μm (45%), PU 10 μm (86%), Medical film 100 μm (73%), Strain gauge 120 μm (27%), Electroless plating (100%) (Table S3).
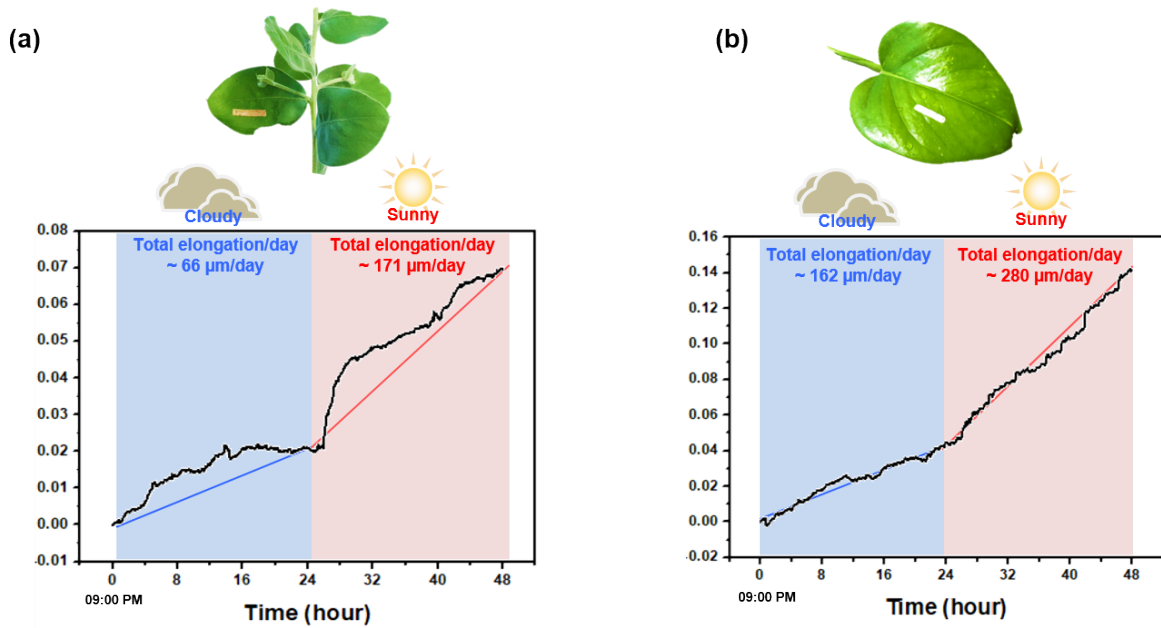
Figure S11. Comparison of plant growth according to weather changes (a) hairy leaf, (b) smooth leaf

Hairy leaf (Figure S11a) and smooth leaf (Figure S11b) real-time measurements were performed continuously for 48 h, sufficient time to see micrometer height reflecting growth rate. In addition, we selected cloudy days and consecutive sunny days and compared the data to confirm the change in the growth rate due to environmental changes. Both plants showed 2.5 and 1.7 times greater growth rates on sunny days than on cloudy days, respectively, indicating that the growth rate of plants can be measured even with environmental changes.
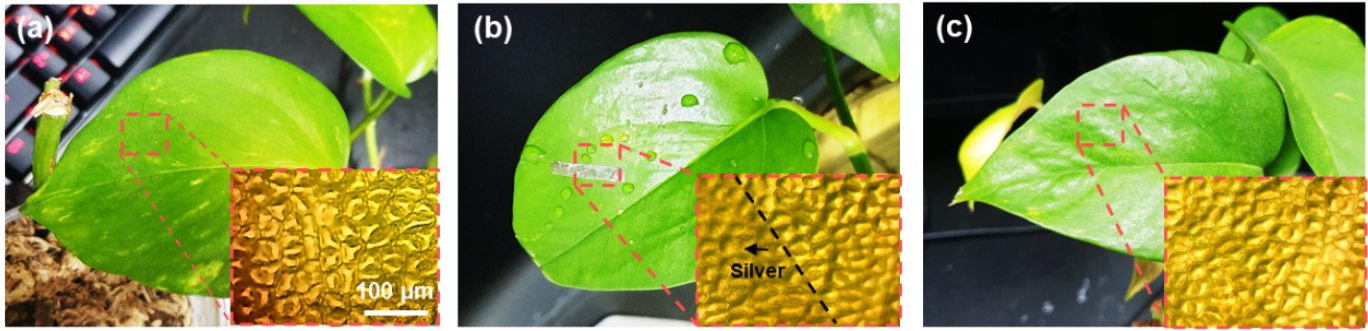
Table S4. Resistance Values of the CS Sensor on Plant Over a 7-Day Period

	1 day	2 day	3 day	4 day	5 day	6 day	7day
Resistance (Ω)	1.6	2.2	2.9	3.6	4.2	4.6	5.1

Figure S12. (a–c) Study of the biological effect of the leaf sensor on leaves.

Figure S12 presents the state of the plant before and after the formation of Ag using $AgNO_3$ and the subsequent sensor attachment. Representative images before sensor attachment can be seen in Figure S12a, the attached sensor in Figure S12b, and the state after sensor attachment in Figure S12c. Even after the removal of the sensor, there was no noticeable effect on the pore size or density of the leaf, and no residual silver was observed.

Additionally, the resistance of the sensor fabricated on the plant using Ag was monitored over a period of 7 days. The observed resistance values are presented in Table S4. The residual solution primarily contains sodium nitrate and excess reagents. To address the potential impact of residual materials on plants, we conducted additional tests to ensure their safety. After the plating process, the plants were thoroughly rinsed with deionized water to remove any residual chemicals. We monitored the plants for any signs of phytotoxicity or adverse effects over a seven-day period and observed no noticeable changes in growth patterns, leaf morphology, or

overall health. This indicates that the residual materials from the plating process do not have a significant impact on plant health when properly managed[2,3].

[1]   H. Jeon, S. K. Hong, M. S. Kim, S. J. Cho, G. Lim, ACS Appl. Mater. Interfaces 2017, 9, 41712.

[2]   K. Song, D. Zhao, H. Sun, J. Gao, S. Li, T. Hu, X. He, BMC Plant Biol. 2022, 22, 323.

[3]   S. R. Ibraheem, I. . Al-Ogaidi, H. F. Al-Azawi, Int. J. DRUG Deliv. Technol. 2022, 12, 1537.

[4] Peng, Zhilong, et al. "Peeling behavior of a viscoelastic thin-film on a rigid substrate." International Journal of Solids and Structures 51.25-26 (2014): 4596-4603.